ACS OMEGA

Open Access

http://pubs.acs.org/journal/acsodf

Article

Polymeric (Poly(lactic-*co*-glycolic acid)) Particles Entrapping Perfluorocarbons Are Stable for a Minimum of Six Years

Alvja Mali,[†] Navya U. Nayak,[†] Jessie van Doesburg, Remco Fokkink, Koen van Riessen, Robbin de Kruijf, and Mangala Srinivas*

Cite This: *ACS Omega* 2025, 10, 6768−6779

Read Online

ACCESS | Metrics & More | Article Recommendations | Supporting Information

ABSTRACT: Polymeric particles, particularly poly(lactic-*co*-glycolic acid) nanoparticles (PLGA NPs), have gained widespread utility in drug delivery, including their incorporation into established clinical formulations. However, their significance is enhanced when loaded with perfluorocarbons (PFCs). This integration enables precise *in vivo* imaging and quantification using advanced techniques such as ^{19}F nuclear magnetic resonance (NMR) or magnetic resonance imaging. These PFC-loaded nanoparticles offer substantial biomedical advantages, including quantitative *in vivo* cell tracking and trackable drug delivery. It is imperative to develop a stable nanoformulation with well-characterized parameters (size, PDI, and PFC content) to facilitate their translation into clinical trials. Another crucial aspect related to their clinical translation is the need for practical storage conditions that are convenient for clinical handling and long-term storage. This study provides compelling evidence of the exceptional long-term stability of PLGA−PFCE (perfluoro-15-crown-5-ether) NPs synthesized via a single-oil-in-water method. When stored at −20 °C, these NPs exhibit remarkable stability for over 6 years. Furthermore, our investigations extend to the behavior of the NPs in powder and suspension forms, demonstrating resilience even after enduring multiple freeze−thaw cycles. Additionally, we explore their stability under various conditions, including water and culture medium, revealing robustness at 4 °C, room temperature (RT), and 37 °C for up to 30 days.

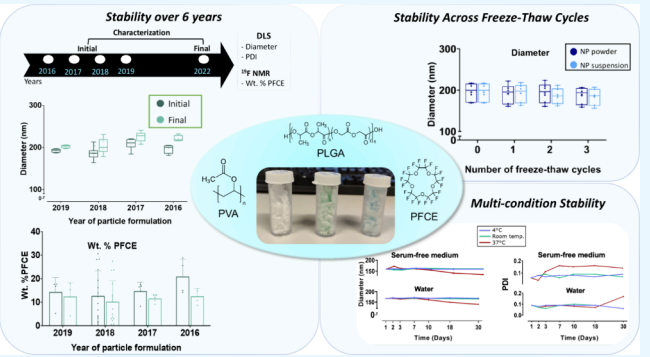

INTRODUCTION

Perfluorocarbons (PFCs) are versatile organic compounds where hydrogen atoms are replaced with fluorine, enabling their use in various applications. Their use as tracers in ^{19}F-MRI provides cutting-edge methods for precise cell tracking.[1−3] This imaging approach provides invaluable data on cell localization and quantification. PFCs exhibit remarkable stability due to their chemical inertness,[4] resisting enzymatic digestion[5] and degradation due to the stabilization of their C−C backbone by highly electronegative fluorine atoms.[6] Upon extended liver retention, PFCs are exhaled from the body,[7] facilitated by their fluorophilic nature, which distinguishes them from hydrophobic or hydrophilic compounds and contributes to their stability. Moreover, PFCs have a unique property known as the "fluorous effect",[8] which causes them to form separate phases due to interactions between their fluorine atoms. Furthermore, different PFCs are selected for ^{19}F MRI based on their molecular weight, carbon chain length, and structure, affecting their biological half-life, exhalation rate, and signal properties. Common examples include perfluoro-15-crown-5-ether (PFCE) for its strong, single resonance peak but prolonged retention, and perfluorooctyl bromide (PFOB), which clears faster but requires higher concentrations due to multiple resonance peaks. Other PFCs, like perfluorodecalin (PFD) and hexafluorobenzene (HFB), are valued for their oxygen sensitivity and favorable imaging characteristics.[8] Indeed, in addition to their role as contrast agents, PFCs demonstrate promise as oxygen carriers,[9] with applications in oxygen delivery.[10] However, to fully realize their clinical potential, researchers are exploring various strategies to address challenges such as fluorophilicity, low surface tension, poor clearance profiles, and the need for suitable in vivo formulations. These include emulsification or incorporation of PFCs into polymeric or lipid nanoparticles, crucial for overcoming their immiscibility with organic and inorganic solvents.

Fluosol (Green Cross Corporation, Osaka, Japan) was the first lipid nanocarrier encapsulating PFC approved by the Food and Drug Administration (FDA) in 1990 for high-risk

Received: September 25, 2024
Revised: December 29, 2024
Accepted: January 13, 2025
Published: February 11, 2025

coronary angioplasty as an oxygen delivery agent.[4] However, the product was withdrawn from the market due to its limited efficacy, technical complexities in usage, and the emergence of superior angioplasty catheters.[11] Fluosol's primary limitation was instability, struggling to maintain a liquid state for over 8 h.[12] Additionally, the need for continuous storage at freezing temperatures limited Fluosol's use in emergencies,[13] as time was required for thawing and sonication before it could be used, which delayed immediate application.[10,14]

Subsequently, new-generation products were developed to address the instability of Fluosol-DA, such as Oxygent (Alliance Pharmaceutical Corp., San Diego, CA) and Oxyfluor (HemaGen, St. Louis, USA).[15] These newer emulsions offer significantly improved stability and user-friendliness, eliminating the need for freezing storage and shipment, with standard refrigeration temperatures being adequate. For instance, Oxygent has a 24-month shelf life when stored at typical refrigeration and can remain stable at room temperature (RT) for several weeks.[16−18] Similarly, Oxyfluor can be stored at RT for over a year.[19]

Another currently commercialized product for oxygen delivery is ABL-101, developed by Aurum Biosciences (Glasgow, UK). It is a third-generation intravenous PFC emulsion for acute ischemic stroke diagnosis and therapy, proven effective for ^{19}F MRI.[20] The emulsion's stability is assured for four years under specific conditions: specific gravity (1.25−1.35), osmolality (280−400 mOsm/kg), and particle size (≤600 nm for 90% and ≤300 nm for 50% of particles) when refrigerated.

For nearly two decades, lipid-based nanoparticles encapsulating PFCs have been studied as contrast agents Ahrens et al.[21] proposed the first successful nanoemulsion (NE) in 2005 for tracking dendritic cells (DCs) using ^{19}F-MRI after ex vivo cell labeling. After several optimizations, the formulation was a source of inspiration for the synthesis of similar commercially available preparations known as Cell Sense (e.g., CS-1000), patented as an MRI tracking agent,[22,23] which gained FDA approval for human clinical trials in 2011.

Furthermore, based on a limited number of published studies, this emulsion has been tested for stability for a maximum of 200 days (approximately six months), revealing an increase in diameter over time.[24] However, stability at RT was much shorter and lacked uniformity in size. An alternative to commercially available NEs is the formulation described by Flögel et al.[25] When stored at 6 °C for 10 weeks, this formulation showed no change in size and zeta potential.

Stability is crucial for the storage and functionalization of nanovectors, which broadens their range of potential applications. Ideal systems should withstand freeze−thaw cycles and allow on-demand modification after prolonged frozen storage. As highlighted by Kramer et al.,[26] lipid-based NE encapsulating PFCs lack stability when frozen at −80 °C and subsequently thawed at 4 °C, especially without PEG-phospholipids. However, lyophilization is not a possible solution because of coalescence, particularly concerning for PFC-NEs due to high PFC vapor pressures.

A prominent degradation mechanism of NEs is Ostwald ripening, a phenomenon driven by the chemical potential within droplets. This leads to the gradual enlargement of larger particles at the expense of smaller ones, posing a challenge in formulation stability. While surfactant choice, emulsification methods, and PFC structure can mitigate Ostwald ripening, complete prevention is challenging. PFC structure plays a crucial role in influencing the rate of Ostwald ripening. Indeed, recent research indicates that perfluorodecalin leads to smaller droplets and slower growth compared to n-perfluorohexane due to differences in solubility and diffusion coefficients.[27] Additionally, longer-chain and branched PFCs yield more stable emulsions.[28−30] Another mechanism of instability is coalescence, which occurs when the surfaces of two nanoemulsion droplets form a contact phase to create a bigger droplet. Although coalescence can be diminished by introducing surface charge and the overall stability of a nanoemulsion can be improved by adding a stabilizer, eventual breakdown or aging of emulsions is inevitable.

To address these stability challenges associated with PFC emulsions, researchers have explored various strategies. Liquid PFCs are commonly introduced as emulsions stabilized with surfactants; however, their colloidal stability remains relatively low, especially at the elevated concentrations necessary for effective cell loading, leading to organ accumulation and suboptimal biodistribution.[42] Enhancing emulsion stability has involved the incorporation of stabilizing agents such as phospholipids and poloxamers. Phospholipids, while effective, are susceptible to hydrolysis and oxidation, compromising long-term stability. Conversely, poloxamers can create highly viscous dispersions, affecting ease of handling and administration.[43] In light of these limitations, encapsulating PFCs within alternative carriers such as polymeric nanoparticles have gained attention.

In terms of long-term stability, an interesting alternative to lipid-based PFC NEs are polymeric nanoparticles (NPs). One of the most used polymers to entrap PFCs is poly(lactid-*co*-glycolic acid) (PLGA), which is clinically approved by the FDA and European Medicine Agency (EMA) as a part of drug delivery systems[7] and exhibits minimal toxicity in these systems.[31] For instance, Srinivas et al.[32] formulated PLGA-based nanoparticles encapsulating perfluoro-15-crown-5-ether (PFCE) and the dye IC-Green [Akorn Inc., IL, USA], enabling diverse imaging modalities including ultrasound, photoacoustic,[33] PET, SPECT,[34,35] and ^{19}F MRI. These PLGA−PFC particles have facilitated cell tracking via ^{19}F MRI[32,33,36−38] over the past decade, with Good Manufacturing Practice (GMP) approval for clinical cell tracking in melanoma patients (ClinicalTrials.gov Identifier: NCT02574377). Importantly, these particles exhibit a significantly faster clearance rate, with a 15-fold reduction[33,39] in half-life compared to core−shell nanoparticles and single-core lipid-based PFC emulsions, because of their multicore internal structure.[40,41] Importantly, these agents are produced as a dry powder, not an emulsion.

Our study aims to demonstrate the enhanced stability of PLGA−PFCE NPs, focusing on specific parameters (i.e., size, PDI, and PFCE content). Findings establish that these particles maintain stability for at least six years after lyophilization. Dynamic Light Scattering (DLS) was employed to measure diameter and PDI values. Additionally, multiangle DLS was used to ascertain particle shape and confirm DLS data, while ^{19}F NMR was employed to quantify the encapsulated amount of PFCE within the particles. Overall, polymeric nanoparticles, because of the lyophilization process, are more convenient.

METHODS

Materials. Poly(D,L-lactide-*co*-glycolide) (PLGA) resomer RG 502H, lactide:glycolide molar ratio 50:50, was obtained

https://doi.org/10.1021/acsomega.4c08663
ACS Omega 2025, 10, 6768−6779

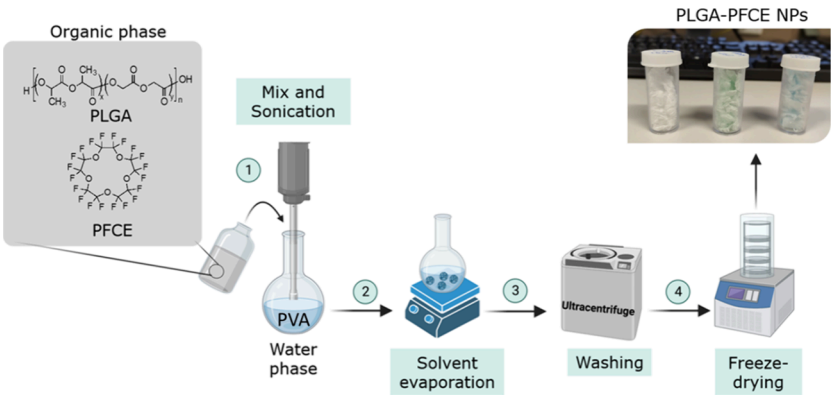

Figure 1. Formulation of PLGA−PFCE particles using single oil-in-water emulsion. The organic phase, containing PLGA and PFCE, is emulsified in an aqueous PVA solution. After emulsification, the NPs are washed, collected by centrifugation, and finally lyophilized. The photo shows how the lyophilized nanoparticles look: the left vial contains particles without dye, while the vials on the right display particles loaded with fluorescent dyes for visualization (not used in this paper).

from Evonik Industries AG, Essen, Germany. Poly(vinyl alcohol) (PVA, 9000−10000 Mw, 80% hydrolyzed), dichloromethane (DCM) (Sigma-Aldrich), deuterium oxide, and trifluoroacetic acid (TFA) were purchased from Sigma-Aldrich (St. Louis, MO, USA). Perfluoro-15-crown-5 ether (PFCE) (Exfluor, Texas, United States). Water was purified by a "pure lab chorus" water purification system from Elga.

Formulation of PLGA−PFCE Nanoparticles. PLGA−PFCE nanoparticles were synthesized using the oil-in-water emulsion method as described in ref 32 and schematically represented in Figure 1. Briefly, PLGA (100 mg) was dissolved in 3 mL of DCM, followed by the addition of 900ul of PFCE. This mixture was premixed with a pipet and added rapidly to 25.5 g of aqueous solution of PVA (1.96 wt %) and emulsified using a sonicator (Sonifier 250; Branson Sonic Power, Danbury, CT, USA) at 40% amplitude for 3 min. Emulsification was followed by overnight solvent evaporation at 4 °C. Next, the particles were collected by centrifugation (16098 rcf, 35 min, 4 °C) and washed three times with deionized water. The particles were then subjected to lyophilization for three to 4 days using a freeze drier to obtain the final product as nanopowder.

Dynamic Light Scattering (DLS). Particles formulated in 2016 (n = 4), 2017 (n = 6), 2018 (n = 16), and 2019 (n = 4) at a concentration of 0.1 mg/mL were characterized in terms of diameter and PDI using DLS (Zeta Sizer-Nano, Malvern Panalytical Ltd., the UK) at a scattering angle of θ = 173° using disposable cuvettes. The particles were measured immediately after formulation (referred to as "initial characterization") and then again in 2022 (referred to as "final characterization"). The values are the intensity mean of four independent measurements of each six runs of 10 s (at 25 °C). For resuspension, we used a standard procedure in which the lyophilized powder was hydrated by adding the appropriate buffer or water, followed by vortexing for a few seconds. If the powder was not fully resuspended, we gently pipetted up and down to further disperse the particles.

Nuclear Magnetic Resonance (^{19}F NMR) Spectroscopy. To quantify fluorine content, PLGA−PFCE NPs were characterized by ^{19}F NMR spectroscopy. For this purpose, a defined content of the nanoparticles was resuspended in 500 uL of D_2O (deuterium oxide) and mixed with 100 uL 1 vol % trifluoroacetic acid (TFA), as an internal reference. The solution was then transferred into 5 mm NMR tubes and measured using a Bruker Avance III 400 MHz NMR spectrometer equipped with a BBFO + probe. Quantitative ^{19}F NMR was measured using an interscan relaxation delay of 25 s and a total of eight scans for enhanced signal averaging. Data analysis was carried out using Mestrenova 14.3.0. To calculate the weight percentage (wt %) of PFCE, the integration of the TFA peak at −76 ppm is first determined and set to one by the software, as it corresponds to a known amount. The software then provides the integration value for the PFCE peak at −92 ppm based on this standard. To derive the total number of fluorine atoms in the PFCE integration, the integration value for PFCE is multiplied by the moles of fluorine atoms in TFA, which is calculated by multiplying the known moles used by 3. This product is then divided by the integration value of TFA. The resulting value is divided by 20, the number of fluorine atoms per PFCE molecule, to obtain the moles of PFCE. Finally, the weight percentage (wt %) is calculated by dividing the mass of PFCE (in grams) by the specific amount of nanoparticles weighed for the ^{19}F NMR measurement and multiplying by 100.

Multi-angle DLS. Multi-angle DLS was performed to determine the shape of PLGA−PFCE particles. These measurements were performed on an ALV instrument equipped with a 22 mW Uniphase Model 1145P HeNe-laser operating at 632.8 nm and an ALV/Dual High QE APD Detector Unit with a fiber splitting device for two detectors connected to an external ALV7004 Multiple Tau Digital Correlator (ALV-Laser Vertriebsgesellschaft m-b.H., Germany). The concentration of samples was 0.01 mg/mL in Milli-Q water. The intensity autocorrelation function, $g_2(\tau)$, and total averaged scattered intensity were recorded for five runs per angle, each lasting 10 s, from 30° to 130° in increments of 5°.

The multi-angle DLS data was analyzed by plotting the decay rate Γ (taken from the first, second, and third order cumulant) as a function of q^2, with q as the wave vector. We calculated the diffusion coefficient from the slope and substituted it in the Stoke-Einstein equation, which is valid for spherical particles to obtain the particle's radius. PDI is the average obtained from the second-order cumulant.

Freeze−Thaw Cycles. Batches of particles (n = 6) were subjected to three freeze and thaw cycles as powder and in suspension. In the case of suspension, particles were dispersed at a 10 mg/mL concentration in ultrapure water. After each

https://doi.org/10.1021/acsomega.4c08663
ACS Omega 2025, 10, 6768−6779

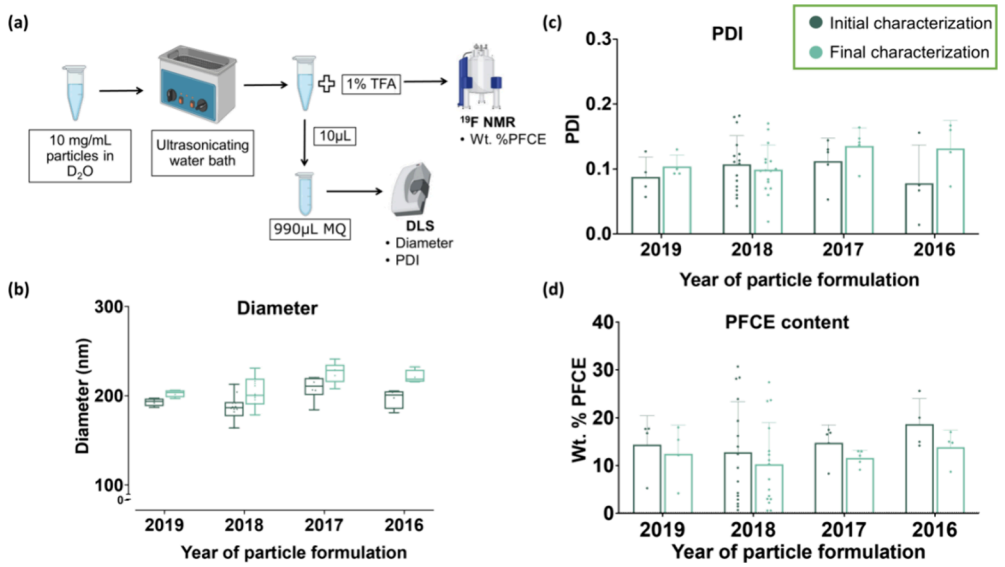

Figure 2. (a) Experimental setup. (b–d) Batches of particles from 2016, 2017, 2018, and 2019 were characterized postproduction and recharacterized in terms of diameter, PDI, and PFCE content in 2022. Effect of time on (b) diameter, (c) PDI, and (d) PFCE content with no prominent difference.

freeze and thaw cycle, DLS was performed, as explained previously, to assess particle diameter and PDI. As described in the previous section, ^{19}F NMR was performed to compare initial PFCE encapsulation and after the completion of three freeze–thaw cycles.

Stability at Different Temperatures (RT, 37 °C, and 4 °C). To assess the colloidal stability of PLGA–PFCE particles, a set of samples (n = 3) were subjected to storage under six different conditions. Each sample was resuspended either in ultrapure Milli-Q water or serum-free media (Dulbecco's Modified Eagle Medium DMEM, ThermoFisher Scientific) at 10 mg/mL. The suspensions were divided and stored at 4 °C, RT, and 37 °C for 30 days. Throughout this month, changes in diameter and PDI were monitored using DLS, employing the same settings as detailed in the previous section.

Transmission Electron Microscopy (TEM). TEM analysis was conducted on PLGA–PFCE samples from 2016, 2017, 2018, 2019, and 2022, along with a control sample from 2024 and PLGA nanoparticles without PFCE. It is important to note that this analysis was conducted two years after (2024) the other experiments (2022), so storage times differ accordingly. Samples were dispersed at 5 mg/mL in Milli-Q water using vortexing and gentle up-and-down pipetting. For TEM imaging, 5 μL of the well-mixed specimen was applied to a Formvar/carbon-coated copper grid and incubated for 2 min at RT. The grid was washed once with 5 μL of Milli-Q water, and negative staining was conducted using 2% uranyl acetate for 30 s at room temperature. The specimen was then dried using blotting paper and air-dried. TEM imaging was performed using a JEOL JEM1400 operating at 120 kV.

Particle Size and Area Analysis. Transmission electron microscopy (TEM) images of nanoparticles were analyzed for particle size and area using ImageJ software (version 1.54f, NIH). JPEG images were converted to 8-bit grayscale for standardization, followed by contrast enhancement (saturation: 0.35%) and noise reduction using a median filter (radius: 2 pixels). Particle edges were enhanced with a Difference of Gaussian (DoG) filter (Gaussian blur sigma: 2), and background subtraction was applied using a rolling ball radius of 50 pixels. Thresholding with the default ImageJ method was followed by binarization and morphological operations, including hole filling, opening, and closing, to refine particle segmentation. A watershed algorithm was optionally used to separate overlapping particles. Particle area and Feret's diameter (in pixels) were measured and converted to nanometers using a scale factor of 5 nm/pixel. Results were exported as tab-delimited text files for statistical analysis. Thresholded masks were merged with original grayscale images to verify segmentation accuracy, and both masks and merged images were saved as TIFF files.

RESULTS AND DISCUSSION

We conducted a comprehensive stability assessment of multicore PLGA–PFCE nanoparticles over a six-year period. These nanoparticles were synthesized using a mini-emulsion technique (as visually depicted in Figure 1 and detailed in the Materials and Methods section) and consist of a PLGA matrix loaded with PFCE and stabilized with PVA, with a mean radius of about 100 nm. Following synthesis, they were stored at −20 °C until subsequent use. Additional modifications, such as introducing fluorescent dyes or ^{1}H MRI agents, can be performed if deemed necessary but were not applied in this study.

Initially characterized in the years 2016, 2017, 2018, and 2019, the nanoparticles were recharacterized in 2022 using the same settings to evaluate changes in diameter, polydispersity index (PDI), and PFCE content. The stability of key parameters such as size, PDI, shape, and PFCE content is crucial, as they significantly influence the pharmacokinetics, tissue distribution, and clearance of nanoparticles.[39]

With time, these nanoparticles have undergone comprehensive physiochemical characterization. Notably, the structural configuration was assessed, revealing a distinctive multicore internal structure.[33] In the existing literature, PLGA–PFCE NPs have been described as having a single core–shell structure.[42] One of the primary challenges in the clinical translation of nanomedicines is their physiochemical stability and shelf life.[43] The nanoparticles' size stability significantly

https://doi.org/10.1021/acsomega.4c08663
ACS Omega 2025, 10, 6768–6779

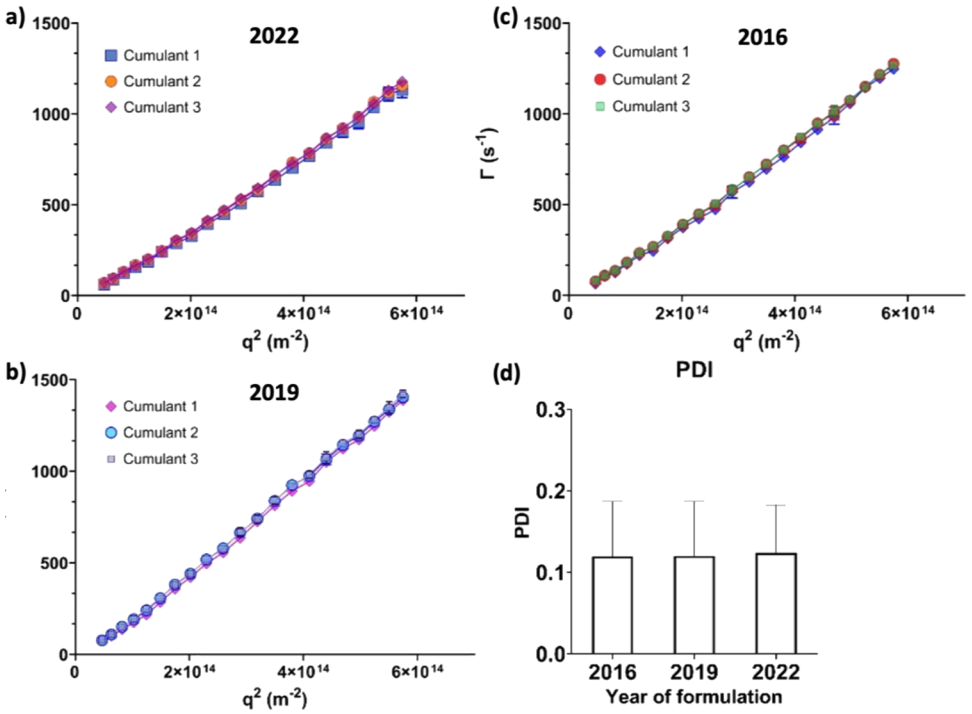

Figure 3. Multi-angle DLS results for PLGA−PFCE particles formulated in (a) 2022, (b) 2019, and (c) 2016. Decay rate Γ (q^2) obtained from the DLS correlation curves by a first (diamond shape), second (circle shape), and third (square shape) cumulant fit. (d) PDI of PLGA−PFCE particles formulated in 2022, 2019, and 2016 obtained from the second order cumulant. Cumulants overlap, indicating shape stability over time.

influences the pharmacokinetics, tissue distribution, and clearance of nanoparticles.[39] In our study, stability entails preserving particle integrity during storage, freeze−thaw cycles, and suspension before injection. Stabilizing agents and material homogeneity play pivotal roles in this aspect.[44] Maintaining low dispersity over time is indicative of thermodynamic stability. We also consider the encapsulated PFCE a critical factor in assessing stability since the encapsulated PFCE is used for quantification in ^{19}F MR imaging applications. Ensuring sustained PFCE retention is pivotal for accurate signal quantification during storage. To thoroughly assess the stability of PLGA−PFCE nanoparticles, initial characterization was performed using dynamic light scattering (DLS). As a result, multicore PLGA−PFCE NPs were characterized in terms of diameter, PDI, and PFCE content (wt %) postformulation in the years 2016 (n = 4), 2017 (n = 6), 2018 (n = 16), and 2019 (n = 4) (Figure 2a). Additionally, recharacterization of the same batches was conducted in 2022 (referred to as final characterization) using the DLS and ^{19}F NMR (examples of ^{19}F NMR spectra from 2016, 2017, 2018, 2019, and 2022 are in Figure S1a−e, respectively) with the same settings. Figure 2b shows that the NPs formulated in 2016, 2017, 2018, and 2019 exhibited an average diameter change relative to measurements conducted in 2022 of 24, 28, 16, and 10 nm, respectively. The average change in PDI (Figure 2c) was found to be 0.05, 0.02, 0.03, and 0.02 for NPs produced in 2016, 2017, 2018, and 2019 respectively. The PFCE content difference between the initial and final characterization was (Figure 2d) by 8% for NPs from 2016, 4% for NPs from 2017 and 2018, while the reduction was 2% for NPs from 2019.

Because intensity-weighted distribution can be skewed by larger particles[45] and number and volume distributions offer insights into particle diameter based on abundance and space occupation, Figure S2 displays the initial and final number (a, d, g, l) volume (b, e, h, m), and intensity (c, f, i, n)- weighted diameter distribution for the years 2019, 2018, 2017, and 2016, respectively. The initial characterization values are plotted over final characterization values in the graphs as average ± SD values of particle diameter of three batches from each year. The SD values are based on the four DLS measurements made per batch. This representation aims to provide a comprehensive understanding of particle diameter across different years. It is noteworthy that PLGA-PFCE NPs displayed surprising stability in terms of diameter and PDI, even after 6 years. The graphical representation of diameter distribution based on number, volume, and intensity (Figure S2a−i) for years 2019, 2018, and 2017 exhibit a remarkable congruence, wherein a discernible overlap is observed between the initial and final characterization. This phenomenon strongly signifies the enduring stability of the polymeric system. Conversely, the diameter distribution graphs for 2016 (Figure S2j−l) display a broader spread in volume and intensity-weighted distributions, shifted toward the right, and thus, a larger diameter. These observations could signify the initial stages of Ostwald ripening processes, wherein smaller particles dissolve in the solution and accumulate into larger particles.[46,47] This process aims to attain a heightened thermodynamically stable state, characterized by a minimized surface-to-area ratio. Moreover, samples from 2016 exhibited a notable decrease in PFCE content (wt %) (Figure 2d), which may have contributed to the initiation of instability processes. However, despite this reduction, the 2016 batches did not show a prominent increase in diameter or PDI (Figure 2b,c). The concentration and type of surfactant are pivotal in preserving the stability of the mini-emulsion. Optimal surfactant concentration, set at 2 wt % for our formulation,[38] enhances the coverage of the interface between the droplet and aqueous phase, stabilizing the emulsion by

https://doi.org/10.1021/acsomega.4c08663
ACS Omega 2025, 10, 6768−6779

Table 1. Diameter (nm) and PDI Obtained from DLS and Multi-angle DLS of PLGA−PFCE NP Batches from 2016, 2019, and 2022 (Control)

		DLS				multi-angle DLS	
year of formulation	name of the batch	initial diameter (nm)	final diameter (nm)	PDI initial	PDI final	diameter (nm)	PDI
2016	A	181	216	0.07	0.17	195	0.12
	B	204	232	0.16	0.16	206	0.14
	C	198	221	0.07	0.07	202	0.11
2019	D	192	202	0.07	0.1	189	0.12
	E	195	206	0.13	0.13	189	0.14
	F	197	197	0.09	0.09	201	0.12
2022	G	208		0.1		203	0.14
	H	218		0.1		213	0.12
	I	221		0.1		209	0.12

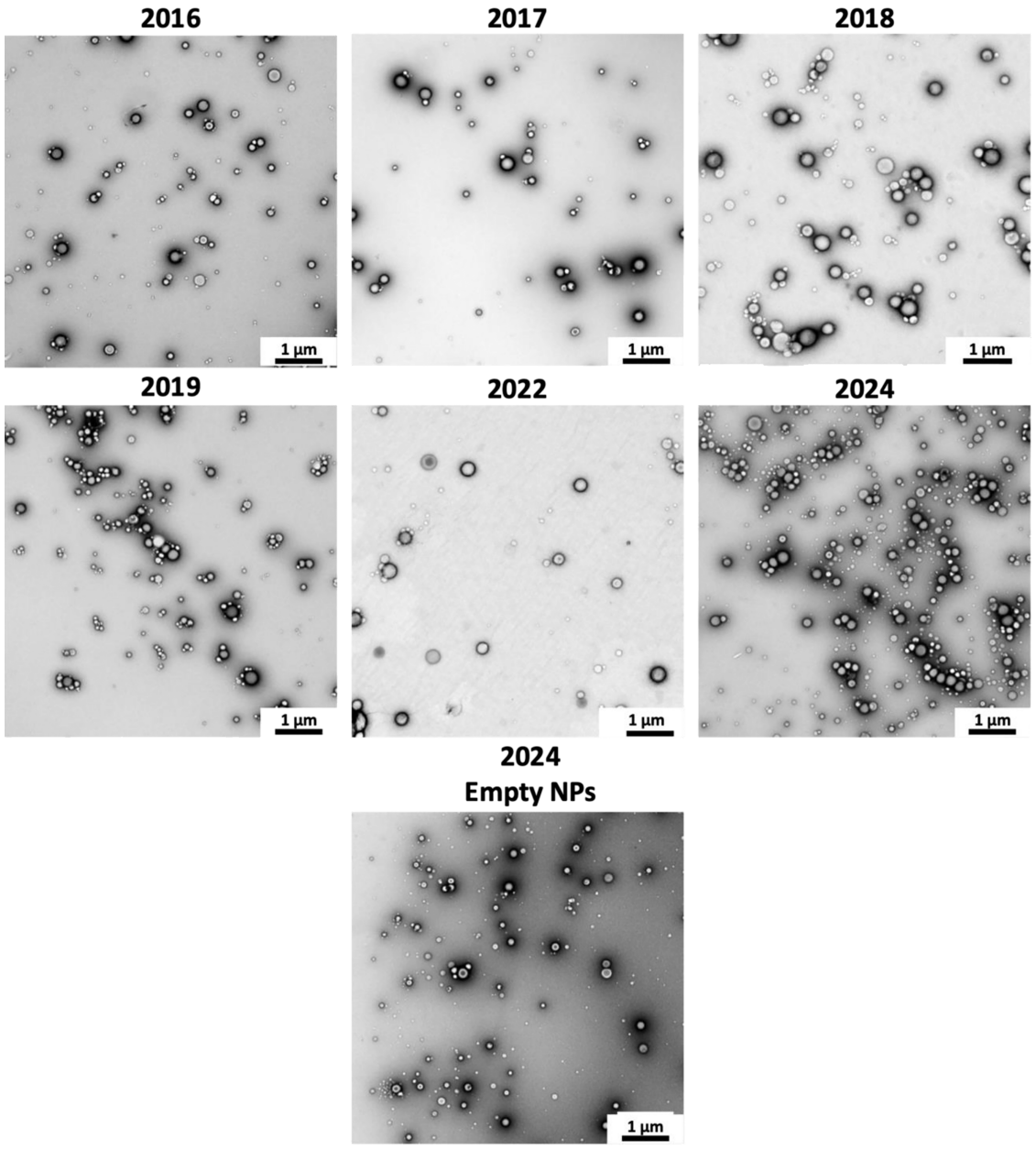

Figure 4. Transmission electron microscopy (TEM) images of PLGA−PFCE NPs from different years of preparation: 2016, 2017, 2018, 2019, 2022, and 2024 and PLGA-only NPs (indicated as Empty NPs). All samples were imaged at 5000× magnification, with a scale bar of 1 μm provided in each panel. The figure illustrates the morphology and stability of PLGA−PFCE NPs over time.

https://doi.org/10.1021/acsomega.4c08663
ACS Omega 2025, 10, 6768−6779

preventing coalescence. Consequently, elevated surfactant levels yield more uniform particles with narrower diameter distribution, reflected in lower PDI values and improved reproducibility. Intriguingly, previous findings from our group have demonstrated that among the commonly used surfactants for PLGA NPs synthesis without PFC, only PVA confers stability.[38] In particular, PVA polymer chains adhere to PLGA NPs through hydrophobic interactions, forming a surrounding layer.[48] When proximity between these coated particles increases in water, the density of PVA chains between them also increases. This prompts the solvent (water) to move from around the particles to the overlapping regions, causing separation. This separation is driven by the polymer chains' higher local pressure and reduced entropy. In simpler terms, the PVA-coated particles repel each other when they are nearby, preventing clumping. This repulsion occurs due to increased pressure between particles and the arrangement of polymer chains.[49]

The DLS measurements shown in Figure 2 were conducted using backscatter detection at 173°, a configuration less sensitive to the presence of larger particles, which tend to scatter light at forward angles predominantly. However, this method does not provide a comprehensive analysis of the samples and is susceptible to over-representation of larger particles. These limitations become particularly relevant when assessing stability.[50] Hence, multi-angle DLS (MDLS) was chosen for analysis. This technique thoroughly assesses the sample's stability concerning diameter, PDI, and shape. The stability analysis included samples from three time points: 2016 (the oldest), 2019 (an intermediate period), and 2022 (the latest), with each time point including three distinct batches for a robust evaluation. At each detection angle, the decay rate Γ of the DLS correlation function is determined by means of cumulant fits. From Figure 3a−c, it can be seen that Γ fitted with the first, second, and third cumulants as a function of the squared wave vector (q^2) gives three overlapping straight lines, showing that the particles retain their spherical shape. Moreover, Figure 3 illustrates a batch from each year, with consistent results observed among the other batches under consideration (Figure S3a−i). PDI values lie around 0.1 (Figure 3d) indicating low dispersity. The slope of the lines corresponds to the diffusion coefficient, further supporting the consistency of particle size and shape.

Table 1 presents the PDI and diameter measurements obtained through both DLS and MDLS analyses for the same set of samples. This comparative analysis was undertaken to validate the reliability of the DLS measurements for our purpose. The DLS measurements indicate a diameter increase from the initial to the final time point. In contrast, MDLS reveals a considerably smaller diameter difference, suggesting greater similarity to the initial measurements. This trend remains consistent across various samples, including those from 2016. Consequently, the utilization of MDLS confirms the robust stability even in batches from 2016, contradicting the initial hypothesis suggesting an early stage of instability, as inferred from the DLS diameter distribution graphs of 2016 batches. Indeed, it is well-known that MDLS offers significant advantages over single-angle DLS. It provides more accurate and reproducible Particle Size Distributions (PSDs), especially for polydisperse and/or multimodal samples. MDLS combines data from different angles for more comprehensive insights into the sample and provides better particle size distribution measurements.[51−53] Moreover, it addresses challenges like the multiscattering effect.[50]

Complementary transmission electron microscopy (TEM) analysis was conducted on PLGA−PFCE NPs from different years of preparation (2016, 2017, 2018, 2019, and 2022), including reference samples from 2024 and empty PLGA NPs (without PFCE), as illustrated in Figure 4 (5000× magnification) and Figure S4 (25000× and 50000× magnification). TEM provided a qualitative assessment of NPs morphology and size distribution over time. Across all years, the NPs retained a spherical morphology with no visible signs of structural degradation compared to the freshly prepared 2024 sample.

The TEM images revealed a range of particle sizes consistent with the size distribution observed in the DLS analysis. This range of sizes is typical for PLGA NPs and was similar for both the 2024 samples and the empty PLGA NPs. Samples from 2017 and 2022 appeared more uniformly dispersed on the TEM grid compared to the others, likely due to differences in sample preparation and imaging conditions, such as particle deposition and the specific imaged area. Despite these variations, the overall consistency in particle morphology and size across the different samples suggests stability over the years of preparation. No significant particle fusion or distinct aggregate formation was observed, further indicating good stability.

The drying process during TEM sample preparation, along with uranyl acetate staining, may lead to particle aggregation. While these artifacts may influence observed dispersity, they do not alter the conclusions regarding particle morphology and structural integrity. The TEM-based size distribution (Figure S5) provides additional insights, confirming particle size stability over time. As expected, TEM-measured diameters were smaller than those obtained by DLS due to methodological differences: TEM measures dried samples, while DLS analyzes hydrated particles in suspension, where the polymer matrix swells due to water absorption. Despite these differences, both techniques confirm stability across the samples. Overall, TEM analysis demonstrates that the PLGA−PFCE NPs retained their structural integrity and morphology over time, aligning with results from other characterization techniques.

In the field of nanoparticle-based products, typically existing as liquid suspensions, stability is a challenge. Indeed, to prevent particles from aggregation, these products need to be kept in cold storage. However, if aggregation occurs, it can jeopardize products' effectiveness and even lead to complications like embolism.[54] Additionally, the presence of water in these suspensions accelerates chemical degradation, undermining both the nanocarrier and the payload through intricate reactions[55] (i.e., medium effect and hydrolytic degradation). For instance, PLGA NPs can gradually release their encapsulated drug due to hydrolysis during prolonged liquid storage.[31] To overcome these challenges, finding ways to keep the nanoparticles stable for a longer shelf life is vital, without needing to store them in cold conditions. In this regard, lyophilization stands out as a powerful approach that tackles these issues comprehensively. By removing water during lyophilization, the random movements of the nanoparticles (Brownian motion) become constrained, thus lowering the risk of particles clumping together during storage. Furthermore, chemical degradation is slowed down in the final solid state.[56] Additionally, the removal of moisture during freeze-drying

https://doi.org/10.1021/acsomega.4c08663
ACS Omega 2025, 10, 6768−6779

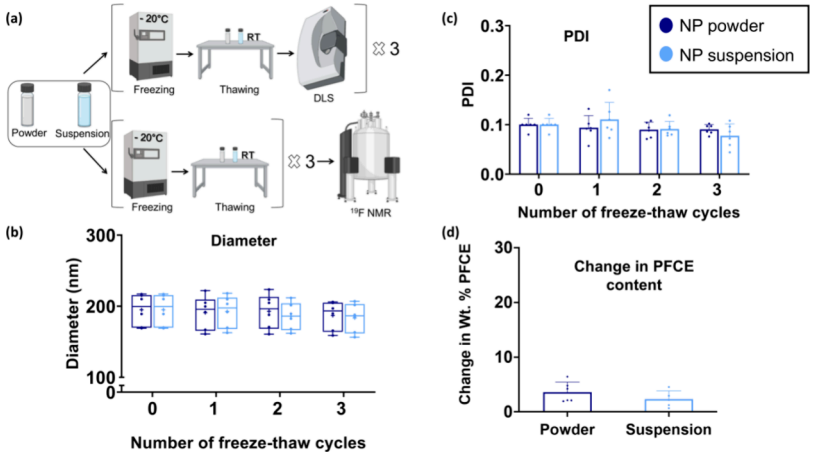

Figure 5. (a) Experimental setup. (b–d) Batches of particles were subjected to three freeze–thaw cycles in their powdered and suspension forms. DLS was performed to measure diameter and PDI after each cycle, whereas the PFCE content was measured initially and after being subjected to all three freeze–thaw cycles. Effect of freeze–thaw cycles on (b) diameter, (c) PDI, and (d) PFCE content, representing no major change in any of the parameters.

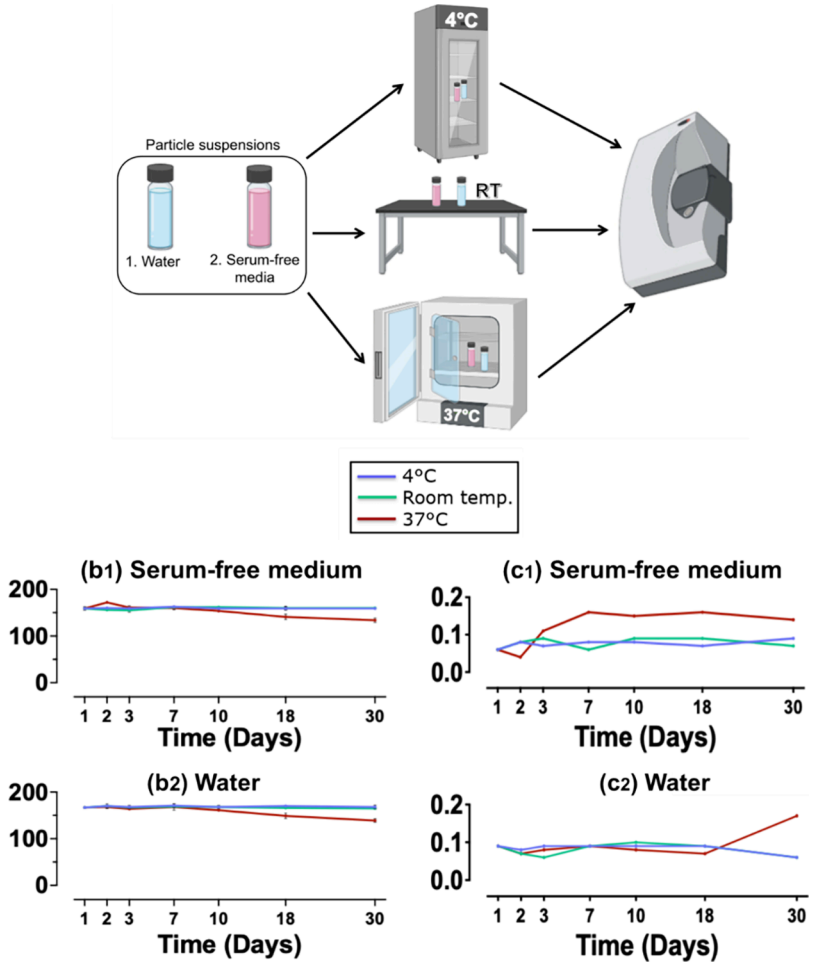

Figure 6. Setup of the experiment (a) and effect of temperature (4 °C, RT, and 37 °C) on the diameter (b1, b2) and PDI (c1, c2) of particles suspended in water and serum-free media for 30 days. The values plotted in the graphs are average ± SD values of particle diameter of the same batch for each condition and time point. The SD values are based on the four DLS measurements made per batch.

eliminates forces driven by surface tension, which would otherwise promote particle aggregation. This drying process further aids in maintaining nanoparticle stability by preventing interactions that typically occur in the presence of moisture.[57] Typically, lyoprotectants are necessary for stability during freeze-drying from both the freezing and drying stresses during processing. However, PLGA NPs present a unique case: stability during freeze-drying can be achieved without lyoprotectants, due to the steric barrier provided by the PVA surface. PVA's hydrophilic layer, featuring exposed hydroxyl

https://doi.org/10.1021/acsomega.4c08663
ACS Omega 2025, 10, 6768–6779

and acetoxyl groups, substantial molecular weight and high surface density mimic a conventional lyoprotectant during freezing. This resemblance allows it to effectively separate particles within the freeze-concentrated phase, preventing direct contact and aggregation.[58] Given the paramount importance of the lyophilization process, we aimed to investigate whether the same stability persists when PLGA NPs encapsulate PFCE. Moreover, considering the significant yield from each produced batch, where we extracted powder multiple times for measurements, we sought to ascertain whether the powder and suspension remained stable after several freeze−thaw cycles. Indeed, PLGA−PFCE NPs are produced in relatively large quantities compared to their experimental requirements. Hence, they undergo repeated freeze−thaw cycles due to their storage at −20 °C. This study was particularly pertinent due to the high vapor pressures of perfluorocarbons, which can result in heightened Ostwald-ripening.[59,60] High vapor pressures make these compounds readily vaporize even at lower temperatures, potentially altering droplet diameter and structure during freeze-drying. PLGA−PFCE particles in the form of powder (n = 6) and suspension (n = 6) were characterized using DLS and ^{19}F NMR after three freeze−thaw cycles (Figure 5a). The six batches were used for both powder and suspension analyses, with each batch being utilized partially for each type of measurement. Notably, PLGA−PFCE NPs exhibited sustained diameter stability throughout the three cycles (Figure 5b). Furthermore, the PDI consistently remained approximately at 0.1, as illustrated in Figure 5c. This remarkable stability was observed in the nanoparticles' powder and suspension forms. Additionally, the loss of PFCE content (Figure 5d) in these NPs in both powder and suspension after three freeze−thaw cycles is minimal, amounting to less than 5% in all the samples. The stability is further confirmed by analyzing the intensity (Figure S6a,b), volume (Figure S6c,d), and number (Figure S6e,f) diameter distribution of each cycle. These graphs represent an average of the six batches used in the experiment, along with standard deviations. The clear overlap of these graphs serves as a strong indicator of the maintained stability.

With the rising participation of nanomedicines in clinical trials, regulatory agencies increasingly require comprehensive physicochemical characterization and a deeper understanding to elucidate how these properties intricately impact biological responses.[61] Indeed, a thorough understanding of nanoparticle properties, particularly their colloidal behavior within biological solutions like cell culture medium, is imperative for evaluating cellular interactions and responses.[62] The possibility for NPs to aggregate introduces potential inaccuracies in results and hampers the reproducibility of experiments, as it alters cellular uptake and toxicity profiles.[63−65] In light of these concerns, we investigated our samples' diameter and PDI stability in both water and cell medium (DMEM) over 30 days. The NPs suspended in these biological solutions, specifically water and serum-free medium, underwent storage under three distinct conditions: (1) 4 °C to simulate long-term storage in refrigerated environment, (2) RT to mimic routine handling conditions, and (3) 37 °C to replicate an *in vivo* environment, mirroring the human body's physiological temperature (Figure 6a). Assessing stability at 4 °C holds particular significance, as it reduces wastage in laboratory settings and enhances handling efficiency from a clinical standpoint. Notably, the reconstitution of the particles begins at RT, thus making it a crucial additional condition to study. Furthermore, evaluation at 37 °C emulates the stability within the context of the human body's physiological temperature. Our observation revealed crucial insights regarding the behavior of NPs under different storage conditions and dispersions. PLGA−PFCE NPs (n = 3, Figure 6 and Figure S7) were dissolved in water at both 4 °C and RT and their diameter remained consistently stable with slight fluctuations. The PDI, which indicates diameter distribution uniformity, remained steady, primarily around 0.1 (Figure 6c2). Figure 6b1,c1 illustrates that when these NPs were dissolved in serum-free media and stored at 4 °C and RT, their diameter remained consistent, along with a constant PDI at 4 °C. However, at RT, the PDI exhibited minor fluctuations, potentially attributed to procedural errors, particularly noticeable on day 7. Nonetheless, the PDI consistently hovered around 0.1 in all cases. Notably, Figure S8a−l showcases a significant overlap in the diameter distribution graphs throughout the 30-day study, whether the NPs were initially dissolved in water or serum-free medium and stored at 4 °C or RT, indicating good stability in these conditions over the study period. On the other hand, NPs dispersed in a serum-free medium and stored at 37 °C initially increased in diameter (Figure 6b1), which could be attributed to multiple factors, including procedural variability and the inherent behavior of PLGA nanoparticles. Specifically, this size increase (Figure 6b1) may result from initial water absorption and subsequent swelling of the nanoparticles as they reach equilibrium. While this was the primary factor in our in vitro setup, in vivo conditions could further amplify this effect through the formation of a protein corona. Around day 10, the diameter begins to decrease as the multicore NPs, composed of small core−shell building blocks, each with a PFCE core individually surrounded by a PLGA shell, break down into separate core−shell units (domains). Our research group has observed this phenomenon in previous studies.[33,39] The rise in PDI from day 3 indicates partial aggregation of these smaller domains, a process that appears to be delayed when the same particles are dispersed in water, where partial assembly occurs after 18 days. However, the PDI remains below 0.2 in both cases, within the acceptable range for polymeric NPs. Conversely, NPs dispersed in water and stored at 37 °C remain stable for 7 days but experience a diameter reduction after 7 days. Furthermore, the intensity diameter distribution curve (Figure S8m,n) clearly illustrates our theory on how the NPs degrade into smaller domains. In the serum-free medium, after 7 days, the graph shows reduced intensity, and the curves become broader with a skewness to the right, indicating potential aggregation of these smaller domains. This pattern is also evident in the volume and number diameter distribution graphs (Figure S8o−r). In conclusion, our study demonstrates that PLGA-PFCE NPs exhibit robust stability under storage and handling conditions, specifically at 4 °C and RT, for the duration of our 30-day investigation. The observations at 37 °C should not be interpreted as an indicator of instability. Instead, they provide further insights into the internal structure of our NPs, revealing a multicore structure rather than a core−shell arrangement. This structural distinction carries significant implications for *in vivo* cytotoxicity and half-life, making it a pivotal factor in our ongoing research.[39]

CONCLUSIONS

In the realm of PFC delivery systems, lipid NEs have long been a standard choice. However, concerns regarding their stability

https://doi.org/10.1021/acsomega.4c08663
ACS Omega 2025, 10, 6768−6779

and storage conditions have prompted exploration into alternative options. Our investigation suggests that PLGA NPs offer promising advantages for PFCE encapsulation, demonstrating stability exceeding six years. Additionally, their more straightforward production processes facilitate the transition to clinical applications, as we have previously shown with the continuous-flow production method. The observed stability of these nanoparticles in powder and suspension forms, even after multiple freeze−thaw cycles, is noteworthy. Our study also examines their behavior under various temperature conditions, indicating stability at 4 °C and room temperature in water and serum-free media suspensions. Although some diameter changes are observed when placed in a serum-free medium at 37 °C, these fluctuations are expected due to the internal multicore structure of the nanoparticles, a phenomenon consistent with prior research findings.

Our findings collectively highlight the potential of these nanoparticles as a reliable platform for PFC delivery, potentially challenging the dominance of lipid NEs. This significance lies in several key aspects, including enhanced research efficiency, resource management by facilitating large-scale preparation and reducing material waste, data consistency, and simplified nanotechnology applications. Consequently, our study contributes valuable insights into advancing PFC delivery systems and may have implications for the broader adoption of ^{19}F MRI in clinical settings.

■ ASSOCIATED CONTENT

Data Availability Statement

The data underlying this study are provided in the published article and its Supporting Information. Raw data can be made available upon request.

Supporting Information

The Supporting Information is available free of charge at https://pubs.acs.org/doi/10.1021/acsomega.4c08663.

Figure S1: ^{19}F NMR spectra of PLGA−PFCE nanoparticles for the years 2016, 2017, 2018, 2019, and 2022; **Figure S2**: diameter distribution in terms of number, volume, and intensity for particles formulated in 2019, 2018, 2017, and 2016; **Figure S3**: multi-angle DLS results for PLGA−PFCE NPs formulated in 2022, 2019, and 2016; **Figure S4**: TEM images of PLGA−PFCE NPs from different years of preparation (2016, 2017, 2018, 2019, 2022, and 2024) and empty PLGA nanoparticles (without PFCE); **Figure S5**: TEM-based particle size distribution of PLGA nanoparticles across formulation years; **Figure S6**: size distribution in terms of intensity, volume, and number of PLGA-PFCE particles after each cycle of freeze−thaw; **Figure S7**: effect of temperature (4 °C, RT, and 37 °C) on diameter and PDI of particles suspended in water and serum-free media for 30 days of the additional two batches; **Figure S8**: size distribution in terms of intensity, volume, and number at 4 °C, RT, and 37 °C of particles suspended in water and serum-free media over 30 days (PDF)

■ AUTHOR INFORMATION

Corresponding Author

Mangala Srinivas − *Department of Cell Biology and Immunology, Wageningen University & Research, Wageningen 6708WD, The Netherlands; Cenya Imaging BV, Amsterdam 1052RK, The Netherlands*; orcid.org/0000-0002-3835-1995; Email: mangala.srinivas@wur.nl

Authors

Alvja Mali − *Department of Cell Biology and Immunology, Wageningen University & Research, Wageningen 6708WD, The Netherlands*

Navya U. Nayak − *Department of Cell Biology and Immunology, Wageningen University & Research, Wageningen 6708WD, The Netherlands*

Jessie van Doesburg − *Department of Cell Biology and Immunology, Wageningen University & Research, Wageningen 6708WD, The Netherlands*

Remco Fokkink − *Department of Agrotechnology and Food Sciences, Physical Chemistry and Soft Matter, Wageningen University, Wageningen 6700 EK, Netherlands*

Koen van Riessen − *Department of Cell Biology and Immunology, Wageningen University & Research, Wageningen 6708WD, The Netherlands*

Robbin de Kruijf − *Department of Cell Biology and Immunology, Wageningen University & Research, Wageningen 6708WD, The Netherlands; Cenya Imaging BV, Amsterdam 1052RK, The Netherlands*

Complete contact information is available at: https://pubs.acs.org/10.1021/acsomega.4c08663

Author Contributions

[†]Alvja Mali and Navya U. Nayak contributed equally to this work. Alvja Mali and Navya U. Nayak: data curation, investigation, formal analysis, visualization and writing-original draft. Jessie van Doesburg: methodology, experiment execution. Remco Fokkink: validation, writing-review & editing. Koen van Riessen: methodology, preparation of the nanoparticles. Robbin de Kruijf: conceptualization, writing-review & editing. Mangala Srinivas: conceptualization, validation, supervision, and funding acquisition. The manuscript was written through contributions of all authors. All authors have given approval to the final version of the manuscript.

Funding

This project has received funding from the European Union's Horizon 2020 Research and Innovation Program under the Marie Sklodowska Curie grant agreement no. NOVA-MRI (859908). The authors acknowledge the funding from ERC-2014-StG-336454-CoNQUeST, TTW-NWO open technology grant STW-14716, ERC-2015-PoC-713524-CONQUEST, ERC-2019-PoC-862989-CENYA, ERA-CVD JTC2017-044, Phoenix Consortium (this project has received funding from the European Union's Horizon 2020 Research and Innovation Program under grant agreement no. 953110), and ERC PoC Unusual IV grant.

Notes

The authors declare no competing financial interest.

■ ACKNOWLEDGMENTS

We thank the ORC (Organic Chemistry) group at Wageningen University, especially Barend van Lagen, for facilitating access to NMR instrumentation, and the PCC (Physical Chemistry and Soft Matter) group at Wageningen University for access to Dynamic Light Scattering (DLS) equipment. We also acknowledge Jelmer Vroom for his assistance with TEM images and the Wageningen Electron Microscopy Centre for access to their facilities. Figures were

https://doi.org/10.1021/acsomega.4c08663
ACS Omega 2025, 10, 6768−6779

created using BioRender.com, and graphs were made using GraphPad Prism.

REFERENCES

(1) Srinivas, M.; Heerschap, A.; Ahrens, E. T.; Figdor, C. G.; de Vries, I. J. M. ^{19}F MRI for quantitative in vivo cell tracking. *Trends Biotechnol.* **2010**, *28* (7), 363−370.

(2) Makela, A. V.; Foster, P. J. Preclinical ^{19}F MRI cell tracking at 3 T. *Magn Reson Mater. Phy* **2019**, *32* (1), 123−132.

(3) Amiri, H.; Srinivas, M.; Veltien, A.; van Uden, M. J.; de Vries, I. J. M.; Heerschap, A. Cell tracking using ^{19}F magnetic resonance imaging: Technical aspects and challenges towards clinical applications. *Eur. Radiol* **2015**, *25* (3), 726−735.

(4) Lowe, K. C. Blood substitutes: from chemistry to clinic. *J. Mater. Chem.* **2006**, *16* (43), 4189−4196.

(5) Ferenz, K. B.; Steinbicker, A. U. Artificial Oxygen Carriers-Past, Present, and Future-a Review of the Most Innovative and Clinically Relevant Concepts. *J. Pharmacol Exp Ther* **2019**, *369* (2), 300−310.

(6) O'Hagan, D. Understanding organofluorine chemistry. An introduction to the C-F bond. *Chem. Soc. Rev.* **2008**, *37* (2), 308−319.

(7) Mansour, H. M.; Sohn, M.; Al-Ghananeem, A.; DeLuca, P. P. Materials for Pharmaceutical Dosage Forms: Molecular Pharmaceutics and Controlled Release Drug Delivery Aspects. *International Journal of Molecular Sciences* **2010**, *11* (9), 3298−3322.

(8) Mali, A.; Kaijzel, E. L.; Lamb, H. J.; Cruz, L. J. ^{19}F-nanoparticles: Platform for in vivo delivery of fluorinated biomaterials for (19)F-MRI. *J. Controlled Release* **2021**, *338*, 870−889.

(9) Krafft, M. P.; Riess, J. G. Perfluorocarbons: Life sciences and biomedical uses - Dedicated to the memory of Professor Guy Ourisson, a true RENAISSANCE man. *J. Polym. Sci. Pol Chem.* **2007**, *45* (7), 1185−1198.

(10) Jagers, J.; Wrobeln, A.; Ferenz, K. B. Perfluorocarbon-based oxygen carriers: from physics to physiology. *Pflugers Arch* **2021**, *473* (2), 139−150.

(11) Winslow, R. M.*Blood Banking and Transfusion Medicine: Basic Principles and Practice-* Blood Substitutes: Basic Principles and Practical Aspects; Elsevier Health Sciences; 2007.

(12) Khan, F.; Singh, K.; Friedman, M. T. Artificial Blood: The History and Current Perspectives of Blood Substitutes. *Discoveries (Craiova)* **2020**, *8* (1), No. e104.

(13) Winslow, R. M. Blood substitutes. *Curr. Opin Hematol* **2002**, *9* (2), 146−151.

(14) Hill, S. E. Perfluorocarbons: Knowledge Gained from Clinical Trials. *Shock* **2019**, *52*, 60−64.

(15) Mohanto, N.; Park, Y. J.; Jee, J. P. Current perspectives of artificial oxygen carriers as red blood cell substitutes: a review of old to cutting-edge technologies using in vitro and in vivo assessments. *J. Pharm. Invest* **2023**, *53* (1), 153−190.

(16) Krafft, M. P.; Riess, J. G. Therapeutic oxygen delivery by perfluorocarbon-based colloids. *Adv. Colloid Interface Sci.* **2021**, *294*, No. 102407.

(17) Keipert, P. E.: Chapter 28 − Oxygent^{TM}, a Perfluorochemical-Based Oxygen Therapeutic for Surgical Patients. In: *Blood Substitutes and Oxygen Biotherapeutics*; Springer 2006.

(18) Riess, J. G.; Krafft, M. P. Chapter 24 − Fluorocarbon Emulsions as in vivo Oxygen Delivery Systems: Background and Chemistry. *Blood Substitutes* **2006**, 259.

(19) Shaw, R. F.; Richard, T. J. Rational Development of Oxyfluor. *Blood Substitutes* **2006**, 298.

(20) Darçot, E.; Colotti, R.; Brennan, D.; Deuchar, G. A.; Santosh, C.; van Heeswijk, R. B. A characterization of ABL-101 as a potential tracer for clinical fluorine-19 MRI. *NMR Biomed.* **2020**, *33* (1), No. e4212.

(21) Ahrens, E. T.; Flores, R.; Xu, H. Y.; Morel, P. A. In vivo imaging platform for tracking immunotherapeutic cells. *Nat. Biotechnol.* **2005**, *23* (8), 983−987.

(22) Ahrens, E. T.; Janjic, J.; Compositions and methods for producing emulsions for nuclear magnetic resonance techniques and other applications. International application; US9352057B2 2009.

(23) Helfer, B. M.; Balducci, A. G.; O'hanlon, C. F., III; Compositions and Methods to Image and Quantify Inflammation. PCT/US1.4/52685; US20160296642A1 2015.

(24) Balducci, A.; Wen, Y.; Zhang, Y.; Helfer, B. M.; Hitchens, T. K.; Meng, W. S.; Wesa, A. K.; Janjic, J. M. A novel probe for the non-invasive detection of tumor-associated inflammation. *Oncoimmunology* **2013**, *2* (2), No. e23034.

(25) Güden-Silber, T.; Temme, S.; Jacoby, C.; Flögel, U. Biomedical ^{19}F MRI Using Perfluorocarbons. *Methods Mol. Biol.* **2018**, *1718*, 235−257.

(26) Kramer, W.; Grapentin, C.; Bouvain, P.; Temme, S.; Flogel, U.; Schubert, R. Rational manufacturing of functionalized, long-term stable perfluorocarbon-nanoemulsions for site-specific ^{19}F magnetic resonance imaging. *Eur. J. Pharm. Biopharm* **2019**, *142*, 114−122.

(27) Freire, M. G.; Dias, A. M. A.; Coelho, M. A. Z.; Coutinho, J. A. P.; Marrucho, I. M. Aging mechanisms of perfluorocarbon emulsions using image analysis. *J. Colloid Interface Sci.* **2005**, *286* (1), 224−232.

(28) Ahrens, E. T.; Zhong, J. In vivo MRI cell tracking using perfluorocarbon probes and fluorine-19 detection. *Nmr Biomed* **2013**, *26* (7), 860−871.

(29) Janjic, J. M.; Ahrens, E. T. Fluorine-containing nanoemulsions for MRI cell tracking. *Wires Nanomed Nanobi* **2009**, *1* (5), 492−501.

(30) Kabalnov, A. S.; Shchukin, E. D. Ostwald Ripening Theory - Applications to Fluorocarbon Emulsion Stability. *Adv. Colloid Interfac* **1992**, *38*, 69−97.

(31) Makadia, H. K.; Siegel, S. J. Poly Lactic-co-Glycolic Acid (PLGA) as Biodegradable Controlled Drug Delivery Carrier. *Polymers-Basel* **2011**, *3* (3), 1377−1397.

(32) Srinivas, M.; Cruz, L. J.; Bonetto, F.; Heerschap, A.; Figdor, C. G.; de Vries, I. J. Customizable, multi-functional fluorocarbon nanoparticles for quantitative in vivo imaging using ^{19}F MRI and optical imaging. *Biomaterials* **2010**, *31* (27), 7070−7077.

(33) Koshkina, O.; Lajoinie, G.; Bombelli, F. B.; Swider, E.; Cruz, L. J.; White, P. B.; Schweins, R.; Dolen, Y.; van Dinther, E. A. W.; van Riessen, N. K.; et al. Multicore Liquid Perfluorocarbon-Loaded Multimodal Nanoparticles for Stable Ultrasound and ^{19}F MRI Applied to In Vivo Cell Tracking. *Adv. Funct. Mater.* **2019**, *29* (19), No. 1806485.

(34) Krekorian, M.; Cortenbach, K. R. G.; Boswinkel, M.; Kip, A.; Franssen, G. M.; Veltien, A.; Scheenen, T. W. J.; Raave, R.; van Riessen, N. K.; Srinivas, M.; et al. In Vivo PET Imaging of Monocytes Labeled with [(89)Zr]Zr-PLGA-NH_2 Nanoparticles in Tumor and Staphylococcus aureus Infection Models. *Cancers* **2021**, *13* (20), 5069.

(35) Krekorian, M.; Sandker, G. G. W.; Cortenbach, K. R. G.; Tagit, O.; van Riessen, N. K.; Raave, R.; Srinivas, M.; Figdor, C. G.; Heskamp, S.; Aarntzen, E. Characterization of Intrinsically Radiolabeled Poly(lactic-co-glycolic acid) Nanoparticles for ex Vivo Autologous Cell Labeling and in Vivo Tracking. *Bioconjug Chem.* **2021**, *32* (8), 1802−1811.

(36) Srinivas, M.; Tel, J.; Schreibelt, G.; Bonetto, F.; Cruz, L. J.; Amiri, H.; Heerschap, A.; Figdor, C. G.; De Vries, I. J. M. PLGA-encapsulated perfluorocarbon nanoparticles for simultaneous visualization of distinct cell populations by ^{19}F MRI. *Nanomedicine-Uk* **2015**, *10* (15), 2339−2348.

(37) Swider, E.; Daoudi, K.; Staal, A. H. J.; Koshkina, O.; van Riessen, N. K.; van Dinther, E.; de Vries, I. J. M.; de Korte, C. L.; Srinivas, M. Clinically-Applicable Perfluorocarbon-Loaded Nanoparticles For In vivo Photoacoustic, (19)F Magnetic Resonance And Fluorescent Imaging. *Nanotheranostics* **2018**, *2* (3), 258−268.

(38) Swider, E.; Staal, A. H. J.; van Riessen, N. K.; Jacobs, L.; White, P. B.; Fokkink, R.; Janssen, G. J.; van Dinther, E.; Figdor, C. G.; de Vries, I. J. M.; et al. Design of triphasic poly(lactic-co-glycolic acid) nanoparticles containing a perfluorocarbon phase for biomedical applications. *RSC Adv.* **2018**, *8* (12), 6460−6470.

(39) Staal, A. H. J.; Becker, K.; Tagit, O.; van Riessen, N. K.; Koshkina, O.; Veltien, A.; Bouvain, P.; Cortenbach, K. R. G.; Scheenen, T.; Flogel, U.; et al. In vivo clearance of ^{19}F MRI imaging

https://doi.org/10.1021/acsomega.4c08663
ACS Omega 2025, 10, 6768−6779

nanocarriers is strongly influenced by nanoparticle ultrastructure. *Biomaterials* **2020**, *261*, No. 120307.
(40) Srinivas, M.; Koshkina, O.; Figdor, C. G.; de Vries, I. J. M.; Process for preparation of beads for imaging. US11286352B2; 2016.
(41) Figdor, C. G.; Vries, D. I. J. M.; Srinivas, M.; Ricondo, L. J. C. Contrast agent and its use for imaging. EP2895201A1; 2012.
(42) Pisani, E.; Tsapis, N.; Paris, J.; Nicolas, V.; Cattel, L.; Fattal, E. Polymeric nano/microcapsules of liquid perfluorocarbons for ultrasonic imaging: physical characterization. *Langmuir* **2006**, *22* (9), 4397−4402.
(43) Hua, S.; de Matos, M. B. C.; Metselaar, J. M.; Storm, G. Current Trends and Challenges in the Clinical Translation of Nanoparticulate Nanomedicines: Pathways for Translational Development and Commercialization. *Front. Pharmacol.* **2018**, *9*, 9.
(44) Cao, G.; Wang, Y. *Nanostructures and Nanomaterials: Synthesis, Properties, and Applications*; World Scientific; 2011.
(45) Nobbman, U.; *Intensity-Volume-Number: Which size is correct?* [https://www.materials-talks.com/intensity-volume-number-which-size-is-correct/] 2017.
(46) Taylor, P. Ostwald ripening in emulsions. *Adv. Colloid Interfac* **1998**, *75* (2), 107−163.
(47) Ravichandran, G.; Yadav, D. N.; Murugappan, S.; Sankaranarayanan, S. A.; Revi, N.; Rengan, A. K. "Nano effects": a review on nanoparticle-induced multifarious systemic effects on cancer theranostic applications. *Mater. Adv.* **2022**, *3* (22), 8001−8011.
(48) Murakami, H.; Kawashima, Y.; Niwa, T.; Hino, T.; Takeuchi, H.; Kobayashi, M. Influence of the degrees of hydrolyzation and polymerization of poly(vinylalcohol) on the preparation and properties of poly(DL-lactide-co-glycolide) nanoparticle. *Int. J. Pharmaceut* **1997**, *149* (1), 43−49.
(49) Tadros, T. F.General Principles of Colloid Stability and the Role of Surface Forces. In: *Colloid Stability*; WILEY-VCH Verlag GmbH & Co. KGaA 2011.
(50) Naiim, M.; Boualem, A.; Ferre, C.; Jabloun, M.; Jalocha, A.; Ravier, P. Multiangle dynamic light scattering for the improvement of multimodal particle size distribution measurements. *Soft Matter* **2015**, *11* (1), 28−32.
(51) Bryant, G.; Thomas, J. C. Improved Particle-Size Distribution Measurements Using Multiangle Dynamic Light-Scattering. *Langmuir* **1995**, *11* (7), 2480−2485.
(52) Bryant, G.; Abeynayake, C.; Thomas, J. C. Improved particle size distribution measurements using multiangle dynamic light scattering 0.2. Refinements and applications. *Langmuir* **1996**, *12* (26), 6224−6228.
(53) Cummins, P. G.; Staples, E. J. Particle-Size Distributions Determined by a Multiangle Analysis of Photon-Correlation Spectroscopy Data. *Langmuir* **1987**, *3* (6), 1109−1113.
(54) Ahire, E.; Thakkar, S.; Darshanwad, M.; Misra, M. Parenteral nanosuspensions: a brief review from solubility enhancement to more novel and specific applications. *Acta Pharm. Sin B* **2018**, *8* (5), 733−755.
(55) Ohtake, S.; Shalaev, E. Effect of water on the chemical stability of amorphous pharmaceuticals: I. small molecules. *J. Pharm. Sci-Us* **2013**, *102* (4), 1139−1154.
(56) Abdelwahed, W.; Degobert, G.; Stainmesse, S.; Fessi, H. Freeze-drying of nanoparticles: Formulation, process and storage considerations. *Adv. Drug Deliver Rev.* **2006**, *58* (15), 1688−1713.
(57) Kasper, J. C.; Friess, W. The freezing step in lyophilization: physico-chemical fundamentals, freezing methods and consequences on process performance and quality attributes of biopharmaceuticals. *Eur. J. Pharm. Biopharm* **2011**, *78* (2), 248−263.
(58) Luo, W.-C.; Beringhs, A. O.; Kim, R.; Zhang, W.; Patel, S. M.; Bogner, R. H.; Lu, X. Impact of formulation on the quality and stability of freeze-dried nanoparticles. *Eur. J. Pharm. Biopharm.* **2021**, *169*, 256−267.
(59) Riess, J. G. Oxygen carriers ("blood substitutes")–raison d'etre, chemistry, and some physiology. *Chem. Rev.* **2001**, *101* (9), 2797−2920.
(60) do Vale Morais, A. R.; do Nascimento Alencar, É.; Xavier Júnior, F. H.; de Oliveira, C. M.; Marcelino, H. R.; Barratt, G.; Fessi, H.; do Egito, E. S. T.; Elaissari, A. Freeze-drying of emulsified systems: A review. *Int. J. Pharm.* **2016**, *503* (1−2), 102−114.
(61) Tinkle, S.; McNeil, S. E.; Muhlebach, S.; Bawa, R.; Borchard, G.; Barenholz, Y.; Tamarkin, L.; Desai, N. Nanomedicines: addressing the scientific and regulatory gap. *Ann. Ny Acad. Sci.* **2014**, *1313*, 35−56.
(62) Moore, T. L.; Rodriguez-Lorenzo, L.; Hirsch, V.; Balog, S.; Urban, D.; Jud, C.; Rothen-Rutishauser, B.; Lattuada, M.; Petri-Fink, A. Nanoparticle colloidal stability in cell culture media and impact on cellular interactions. *Chem. Soc. Rev.* **2015**, *44* (17), 6287−6305.
(63) Albanese, A.; Chan, W. C. W. Effect of Gold Nanoparticle Aggregation on Cell Uptake and Toxicity. *ACS Nano* **2011**, *5* (7), 5478−5489.
(64) Limbach, L. K.; Li, Y. C.; Grass, R. N.; Brunner, T. J.; Hintermann, M. A.; Muller, M.; Gunther, D.; Stark, W. J. Oxide nanoparticle uptake in human lung fibroblasts: Effects of particle size, agglomeration, and diffusion at low concentrations. *Environ. Sci. Technol.* **2005**, *39* (23), 9370−9376.
(65) Wick, P.; Manser, P.; Limbach, L. K.; Dettlaff-Weglikowska, U.; Krumeich, F.; Roth, S.; Stark, W. J.; Bruinink, A. The degree and kind of agglomeration affect carbon nanotube cytotoxicity. *Toxicol. Lett.* **2007**, *168* (2), 121−131.

https://doi.org/10.1021/acsomega.4c08663
ACS Omega 2025, 10, 6768−6779